Potential of a Thin-Film Cell for assessing the Sensitivity of Nickel-Base Alloys to Crevice Corrosion

H. Klinklin, Sabrina Marcelin, Benoît Ter-Ovanessian, M. Monnot, Bernard Normand

Potential of a Thin-Film Cell for assessing the Sensitivity of Nickel-Base Alloys to Crevice Corrosion

H. Klinklin,[1,2] S. Marcelin,[1,z] B. Ter-Ovanessian,[1] M. Monnot,[2] and B. Normand[1]

[1]*Univ. Lyon, INSA Lyon, Université Claude Bernard Lyon 1, CNRS, MATEIS, UMR5510,69621 Villeurbanne cedex, France*
[2]*Centre de recherche des matériaux du Creusot, Industeel, 71200 Le Creusot, France*

Nickel-base alloy 825 is prone to crevice corrosion in seawater. A modified and updated thin-layer cell was used to mimic crevice corrosion, and a new approach to monitor the evolution of the material behavior was developed. The corrosion potential, polarization resistance, and electrolyte resistance were demonstrated to be good indicators to follow the different stages of the crevice-corrosion process. The results were discussed in regard with the cathodic process kinetic. The different tested conditions justify the interest of the methodology developed for this set-up.

Manuscript submitted May 31, 2023; revised manuscript received July 26, 2023. Published August 14, 2023.

Nickel-base alloy (NBA) 625 is well known for its high crevice corrosion resistance in seawater and sour environments. Thus, it is widely used for the cladded pipelines in the petrochemical industry.[1] One of the disadvantages of NBA 625 is its high cost due to the high content in nickel and other alloying elements. The less expensive NBA 825 could be a good candidate to replace NBA 625. However, it is more sensitive to crevice corrosion in seawater.[2,3] Our previous work (internal note) showed that after three months of immersion in natural seawater at 30 °C, no corrosion was observed for the exposed NBA 625 coupon (Fig. 1a), whereas 825 exhibited crevice corrosion for the half of exposed coupons (Fig. 1b). Moreover, from SEM observations, the NBA 825 is characterized by a sensitive intergranular corrosion (Fig. 1c).

Alves et al. observed the same type of behavior for both materials after 9 weeks of immersion in chlorinated water at 50 °C, where NBA 825 was prone to crevice corrosion while the NBA 625 was undamaged.[3] The pitting resistance equivalent number (PREN) for 825 is 33 than for 625 is 52 and according to the NACE standards alloys with a PREN of less than 40 cannot be used in seawater without cathodic protection. Moreover, the critical crevice temperature is 5 °C for NBA 825 and 35 °C for NBA 625 (ISO 188089 standard),[4] which also indicates the highest sensitivity to this type of corrosion of NBA 825. For this reason, some works were done to define new alloys with intermediate composition between 625 and 825 to obtain a material with the required properties at lower cost.[4–6] Botinha et al. have designed a new alloy as a further development of NBA 825 by adding molybdenum and copper.[4,5] The calculated PREN of this new alloy is 42. By modifying the composition of the alloy, the resistance of the chloride induced localized corrosion was improved. Bergstrom et al. have decided on a different development path.[6] They decreased the amount of nickel (balanced by iron) and maintain molybdenum close to 6% weight to preserve a PREN value in excess of 40.

In these studies, the validation of the alloys was done through standardized tests (mainly ASTM G48 C,D and G78[7,8]) and the role of the alloy composition modification on the corrosion mechanisms was not explicitly investigated. Indeed, the most common set-up to study crevice corrosion susceptibility is multiple crevices assembly, which consists of two non-metallic segmented washers with a certain number of confined areas to form one or multiple crevices.[9–14] The torque applied to assemble these washers is a predominant factor affecting the crevice-corrosion initiation, as it will be more likely with higher torques.[9,14] To limit this bias, the crevice corrosion was initiated by confining an electrolyte above the working electrode with an insulating plate so no torque has to be applied.[15,16] With these techniques, metallic materials are often ranked with respect to their susceptibility to crevice corrosion by a statistical count of the number of corrosion sites and their depths obtained at the end of standardized experiments. These observations are generally made post-mortem and do not provide any information on the evolution of the system during the corrosion process. Conversely, few studies follow the evolution of key parameters indicative of the evolution of the interfacial reaction during sample immersion.[17,18] Based on these standardized approaches, it remains a lack of knowledge on the in situ evolution of the system during crevice corrosion.

Other experimental set-ups with tunable confined area are also used. One set-up is the thin-layer cell, which was first developed by Fiaud et al. in 1987 to study the electrochemical behavior of the Fe–36Ni alloy[19] and zinc[20] in confined medium. Later, Gabrielli et al. monitored the thin-layer cell with a platinum micro-electrode with a diameter of 10 μm in a confined environment to estimate the diffusional mass transport on the impedance at low frequencies.[21] Based on the works of Fiaud and Gabrielli, a thin-layer cell was developed by Remita et al. for the study of the corrosion of carbon steel under CO_2.[22] A preliminary work was performed to develop a reliable way to set the parallelism between the top and bottom parts of the device using the measurement of real part of impedance at high frequency under three platinum probes. The originality of such an assembly is in the control of the thickness of the thin film of electrolyte and the geometry of the thin layer. Precaution must be taken when defining the initial electrolyte, which is required to be in physico-chemical conditions close to those for depassivation (to reduce incubation time), and not so severe as to modify corrosion sensitivity or mechanism. Based on Remita's set-up, Marcelin et al. investigated the crevice corrosion of a martensitic stainless steel.[23] The ability of the material to be repassivated has been studied in confined media (the bulk electrolyte was 0.1 M NaCl + 0.04 M Na_2SO_4) for different electrolyte thicknesses ranging from 100 to 800 μm. Thus, a cathodic polarization at −1 V/SCE (Saturated Calomel Electrode) to reduce both dissolved and part of the iron oxides was carried out before the impedance measurement after 17 h of immersion at the corrosion potential. It has been shown that the more severe the confinement, the less the material can repassivate. To get information on the chemistry of the confined environment, polarization curves were plotted in bulk solution for different pH or chloride ion concentration conditions. Critical conditions were identified by a change in the electrochemical behavior of the material from a passive to an active state. In addition, for each condition, the electrolyte resistance was measured and compared to that obtained for the different electrolyte thicknesses in the thin-cell layer. Thus, by these ex situ measurements, it was shown that the pH decreased from 1.5 to 1.1 or that the Cl^- concentration increased from 0.4 to 1.2 M when the electrolyte thickness decreased from 800 μm to 100 μm.[23] These tests provided information on electrolyte changes, but did not accurately determine the critical pH and Cl^- ion concentration.

Based on the knowledge of crevice corrosion mechanisms, the objective of this work is to develop an experimental set-up to

[z]E-mail: sabrina.marcelin@insa-lyon.fr

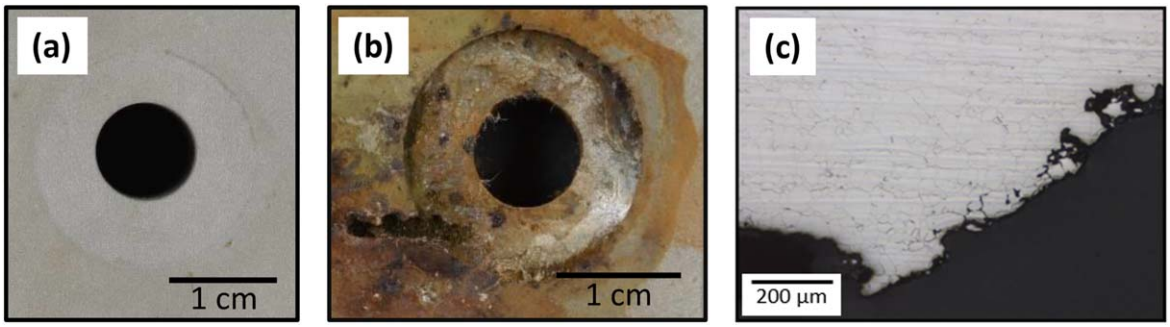

Figure 1. Optical observations of coupons after 3 months of immersion in natural seawater at 30 °C in a multiple crevice assembly for: (a) 625, (b) 825 NBA and (c) SEM detail on the 825 corroded surface.

reproduce the natural deaeration of the confined electrolyte, leading to dissociation of the anodic and cathodic sites. To study the corrosion mechanism linked to physico-chemical changes in the confined electrolyte (pH and chloride concentration), the electrochemical behavior at corrosion potential of the NBA 825 sample is measured with time. The originality of this work is to assess both the chemical modifications of the confined electrolyte and the electrochemical behavior of the alloy in contact with a low stagnant electrolyte volume through open-circuit potential (OCP) and electrochemical impedance spectroscopy (EIS) measurements. A new upgrade of the thin-layer cell based on the work of Marcelin et al.[23] was developed including in situ pH and O_2 sensors to follow the evolution of electrolyte chemistry. First, a preliminary study was done to select a starting electrolyte solution to use in the thin-layer cell to obtain corrosion modes similar to those observed in natural seawater and to initiate crevice corrosion in a reasonable time. Then, the evaluation of the corrosion behavior of NBA 825 is discussed regarding the chemistry modification of the confined electrolyte. Information thus obtained should demonstrate the effect of a change in the chemical composition of alloy 825 on its corrosion resistance under these particular conditions.

Experimental

Material.—The chemical composition of the NBA 825 plates from the Industeel—ArcelorMittal Group is given in Table I. After being cast, the alloy was hot rolled and then heat treated at 950 °C for 10 min before water quenching.

From microstructural analysis, it was observed that the NBA microstructure is characterized by austenitic grains, the presence of inter or intragranular TiN phases and chromium carbides $Cr_{23}C_6$ mainly located at grain boundaries.

Electrochemical measurements.—Before the investigation of the electrochemical behavior of the NBA 825 in a confined medium, a suitable electrolyte was selected. This electrolyte enables the reproduction of corrosion damage patterns at grain boundaries, as observed in previous standard tests in natural seawater, which will form a biofilm on the sample surface (Fig. 1c). Therefore, two different set-ups were used in this study for *(i)* the determination of the chemical stability of the passive film and *(ii)* the electrochemical behavior of the NBA 825 in stagnant and confined environment.

NBA 825 passivation domain.—As the NBA 825 is intended for use in seawater, the support electrolyte was an aqueous solution with a 0.5 M chloride concentration. The near-neutral solution was acidified by the progressive addition of HCl or H_2SO_4. The acidification with HCl has the advantage of avoiding the introduction of extra species not naturally present in seawater to the solution. However, its use increases the chloride concentration at the same time as the acidity, which may modify the corrosion behavior inside the confined area. The electrolyte was also acidified with H_2SO_4 to avoid excess in the chloride content. In contrast, the sulfate ions compete with chloride adsorption as they have better affinity with Fe and Ni than Cl^- ions and will protect the material from the detrimental effect of chlorides.[24] Effectively, sulfate act as an inhibitive specie of crevice corrosion.

Table I. Chemical composition of NBA 825 (in wt%).

Fe	Ni	Cr	Mo	Cu	Ti	Si	Mn
Bal.	40.070	23.223	3.203	1.740	0.728	0.280	0.250
Al	B	W	C	P	Nb+Ta		S
0.112	0.014	0.026	0.013	0.012	0.008		0.003

The effect of the acidifying agent is studied in Effect of the electrolyte composition on the passive properties of NBA 825 section. The tested pH range was 0.05–0.7. The pH was measured using a Mettler Toledo pH meter with an InLab Pure Pro pH probe. All the electrolyte compositions tested are reported in Table II.

A three-electrode set-up was used, with alloy 825 as the working electrode, a platinum counter electrode, and Ag/AgCl 3 M as the reference electrode. The electrochemical cell volume was 300 ml. The working electrode consisted of a rod of 1 cm^2 section that was mechanically polished using SiC papers up to 1200 grade and then successively rinsed with deionized water, ethanol, and acetone in an ultrasonic bath.

To minimize ohmic drop and electrolyte contamination, a Luggin capillary was placed between the reference electrode and the working electrode. For these preliminary tests, the working electrode was pressed against a gasket to ensure the tightness of the system, and an electrical contact was made, allowing the connection to the potentiostat. The chemical stability of the passive state is defined by the depassivation pH (pH_d) below which the material becomes unprotected by its passive film. This critical pH was determined from polarization curves plotted from—50 mV vs OCP to 900 mV vs Ag/AgCl with a sweep rate of 1 mV s^{-1} after 50 min of immersion at the corrosion potential. An Autolab PGSTAT101 potentiostat in combination with NOVA software was used to acquire data.

Electrochemical behavior in confined area.—In the thin-layer cell set-up used to reproduce crevice corrosion, a selected electrolyte was used and the system was maintained at 30 °C for the motivations discussed in Effect of the electrolyte composition on the passive properties of NBA 825 section.

The thin-layer cell developed for this study is presented in Fig. 2. The cell was composed of a support, a bottom part, and a top part (Fig. 2a), allowing the electrolyte thickness between the last two parts to be controlled using a micrometer. The parallelism between the bottom and top part was ensured using several translation stages.

The bottom part consisted of the working electrode, which was a cylinder of 825 NBA (∅ = 15 mm) embedded in resin (∅ = 30 mm). It was polished with SiC paper up to 4000 grade to provide a flat surface. The maximum particle size using P4000 paper is 5 μm.

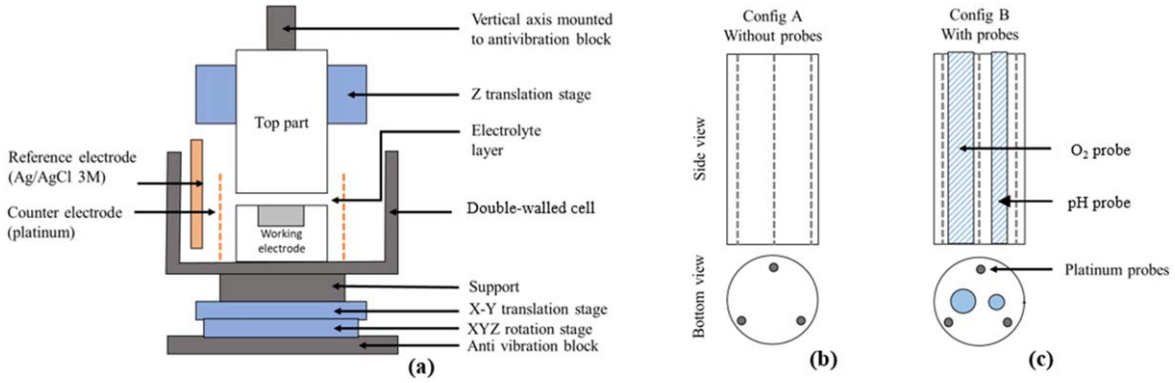

Figure 2. Schematic representation of the thin-layer cell: (a) full view, top parts (b) without and (c) with pH and O_2 probes.

Table II. Electrolyte compositions.

pH	0.70	0.57	0.52	0.50	0.40	0.35	0.30	0.10	0.05
Acid	HCl	HCl	HCl	HCl or H_2SO_4	HCl or H_2SO_4	H_2SO_4	HCl or H_2SO_4	H_2SO_4	H_2SO_4
[acid] in M	0.20	0.27	0.30	0.32	0.40	0.45	0.50	0.79	0.89

Thus, the maximum groove size induced by polishing will be smaller than 10% of the minimal thickness tested (50 μm). Then, the electrode was rinsed with deionized water, ethanol, and acetone in an ultrasonic bath.

The sample was glued on a copper stud using silver coating and a hollow screw was placed in the stud, allowing it to be plugged into the potentiostat. The entire bottom part was embedded in a double-walled cell to enable temperature control of the electrolyte. The cell was placed on two stages to translate the bottom part along the X and *Y* axis and rotate it around XY, XZ, and YZ (Fig. 2a). The top part consisted of a PTFE cylinder ($\varnothing$ = 36 mm) fixed on a stage for vertical displacement to fix the thin-layer thickness. Two different top parts were used: the first one without probes (Fig. 2b) and the second one had two holes to insert an O_2 sensor and a pH sensor in the thin-layer cell (Fig. 2c). The oxygen sensor was a MicroTip - Fiber Optic Oxygen Sensor from WPI composed of a 50 μm-wide optic fiber housed in a syringe with a 1 s response time. The pH probe was a Mettler Toledo in-lab NMR that could measure a pH range from 0 to 14. Its small diameter (3 mm) allowed it to fit into the hole of the top part of the thin-layer cell. To perform electrochemical measurements, an Ag/AgCl reference electrode and a cylindrical counter-electrode in platinum were used.

To guarantee optimal parallelism between the top and bottom parts, three 1 mm diameter platinum disks were embedded in the top part of the cell spaced 120° apart, permitting the electrolyte resistance measurements. From the methodology developed by Remita et al., the parallelism error between the two parts can be minimized, enabling a homogeneous electrolyte thickness at the surface of the working electrode. The comparison of the adimensionnal admittance, defined in[25] obtained from the real impedance measurement at high frequency, ensure that the electrolyte thickness below the three platinum micro-electrodes is equal. The value of parallelism errors ($\delta_{e\ sample}$) is given in Eq. 1:[25]

$$\delta_{e\ sample} = \left(\frac{Z_O - Z_M}{d}\right)_{\max} 2.R_O \qquad [1]$$

With Z_O and Z_M the Z-coordinates of the center of the working electrode (point O) and of the point included in the platinum probes at medium and low position (point M), respectively, d is the distance OM and R_0 the radius of the working electrode.

The electrochemical behavior of NBA 825 in a confined environment was investigated from successive impedance measurements over time at the corrosion potential. This technique was chosen to study the evolution of the passive film. To ensure that the tests are reproductible they were repeated at least three times for each condition. For all experiments, the thickness of electrolyte was 50 μm ± $\delta_{esample}$. The impedance diagrams were recorded from 10^5 Hz to 3×10^{-3} Hz, with 8 pts/decade and with a sinusoidal perturbation around the corrosion potential of 10 mV RMS. Condition of acquisition of impedance diagram were verified for each measurement with Kramers-Kronig relations. The data were acquired with a Ametek PARSTAT 3000 A potentiostat and the software VersaStudio. The fitted parameters were obtained from a recently lab-made open-source software based on the simplex method and Levenberg–Marquardt regression.[26]

Results and Discussion

The effect of the pH and the chloride ion concentration was studied to define the passivity domain of the alloy. Thanks to this preliminary study, a suitable electrolyte was used in the thin-layer cell to allow a reasonable incubation time for a laboratory study. The electrochemical behavior of NBA 825 and the electrolyte chemistry modifications were investigated in the confined area defined by a small volume of electrolyte. The evolution of the interfacial reactions was closely followed to better understand the alloy behavior toward crevice corrosion stages. Finally, the potential of this methodology for characterizing the crevice corrosion behavior of the NBA 825 for different severity conditions will be discussed.

Effect of the electrolyte composition on the passive properties of NBA 825.—From the polarization curves (Fig. 3a) obtained after 50 min at corrosion potential, the depassivation pH (pH_d) can be obtained by plotting the maximal current density as a function of the pH (i_{max} = f(pH) in Fig. 3b). The value was obtained for the alloy immersed under different acidic conditions with HCl and H_2SO_4. When the material was active, the maximum current density was determined as the maximum current density on the activity peak, consistent with the methodology proposed by Crolet et al.[27] For the passive state, the current density of the passive plateau was considered. When acidified with HCl, the maximum current density for similar pH was higher than that when acidified with H_2SO_4. For example, at pH 0.3, the maximum current density of the NBA 825 in the HCl acidified solution was 9.6×10^{-4} A cm^2 compared with that of 2.1×10^{-4} A cm^2 for the H_2SO_4 acidified solution. The pH_d of NBA 825 was determined to be 0.38 for the H_2SO_4 acidified solution

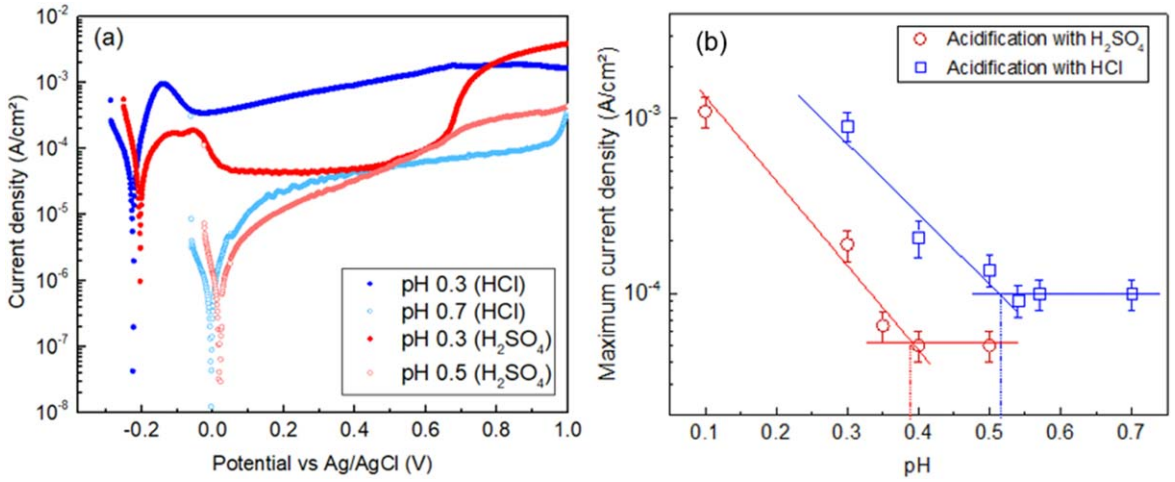

Figure 3. (a) Anodic polarization curves plotted after 50 min at corrosion potential with a sweep rate = 1 mV s^{-1} and (b) maximum anodic current density as a function of the electrolyte pH.

and 0.52 for the HCl acidified solution in 30 g/L NaCl and aerated electrolyte. Acidification with HCl was more severe. This result can be explained by several phenomena. At low pH, the passive film is sensitive to chloride and will become unstable. The passive film breakdown is then favored due to the chemisorption of chlorides on the surface of the passive film.[24]

From these results, the electrolyte selected for the tests in the thin-layer cell was an aqueous solution of 30 g L^{-1} NaCl acidified by H_2SO_4 to obtain an initial pH of 0.5. This concentration of NaCl was selected to replicate the initial chloride concentration in seawater, as explained in the experimental part. The adjusted pH was selected to be slightly above the pH_d (0.38) to attain the aggressive condition leading to the depassivation of the material in a reasonable time. The increase in [Cl^-] in the thin-electrolyte layer was only due to the electromigration of chloride ions from the bulk to the confined environment. Sulfate will also prevent pitting, favored by an important concentration in chloride, and consequently favor the chemical depassivation of the NBA 825.

Monitoring of the different stages of crevice corrosion.—Using the probes inserted in the thin-layer cell (Fig. 2c), the evolutions of dissolved oxygen and pH were monitored during immersion for the NBA 825. The corrosion potential of NBA 825 in a confined environment (NaCl 30 g L^{-1} at pH 0.5) was measured for two thin film electrolyte thicknesses, 200 ± 40 μm and 50 ± 11 μm, as presented in Figs. 4a and 4b, respectively. For both cases, the corrosion potential remained stable for a certain time and sharply decreased to reach a value between −0.19 and −0.30 V vs Ag/AgCl. In parallel, the pH continuously decreased during the immersion to reach 0.22, which is lower than the depassivation pH (Fig. 4a). As shown in Fig. 4b, the dissolved oxygen content also decreased with time and then sharply dropped at the same time as the corrosion potential. These results are consistent with the crevice corrosion mechanism, and it can be underlined that the developed thin-layer cell allows the conditions leading to this type of corrosion to be reproduced: deaeration of the confined area and a decrease of the pH leading to the depassivation of the material. The capability to follow such parameters in the cell is essential to link the evolution of passive properties of the material to the electrolyte chemistry. Figure 4c presents the surface state of the working electrode after 144 h of immersion in the 50 μm-thick electrolyte layer. The corrosion was heterogenous due to the geometrical defect induced by the presence of probes. To avoid such effect, for the rest of the study, the electrolyte was confined between the NBA 825 and the top part without the two probes (Fig. 2b). The interfacial reactions were then investigated using electrochemical impedance measurements to closely analyze the evolution of the local mechanism at the interface between the NBA 825 and confined electrolyte.

Evolution of the electrochemical reactions in the thin-layer cell.—Figure 5 shows the evolution of corrosion potential for the sample in the configuration without probes (Fig. 2b) and for 50 μm ± 26 μm-thick film of electrolyte. The three distinctive stages of crevice corrosion were still observed. During the first 4 days (96 h)

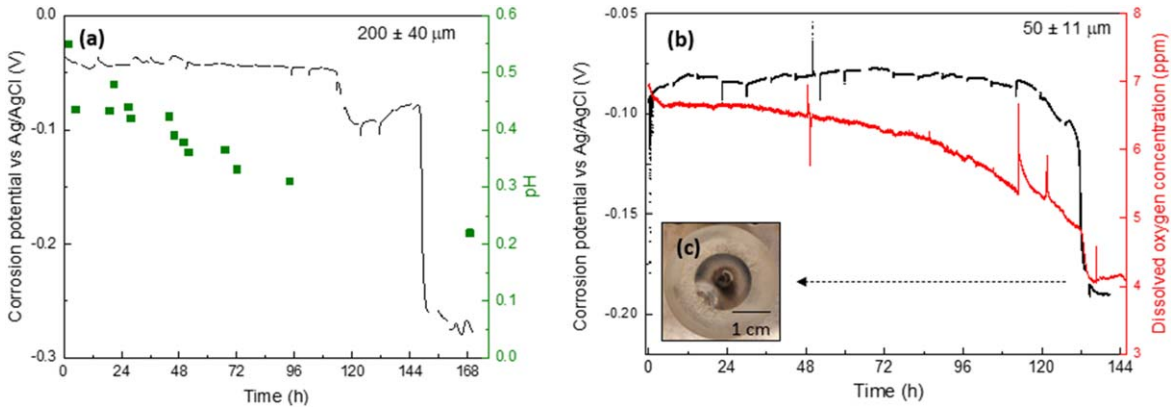

Figure 4. (a) Evolutions of corrosion potential (in black), pH (in green), and dissolved oxygen content (in red) for NBA 825 in contact with a thin layer of electrolyte (30 g/L NaCl acidified by sulfuric acid) of: (a) 200 μm ± 40 μm and (b) 50 μm ± 11 μm. (c) Macrograph of the sample after 144 h of immersion in the thickest electrolyte layer.

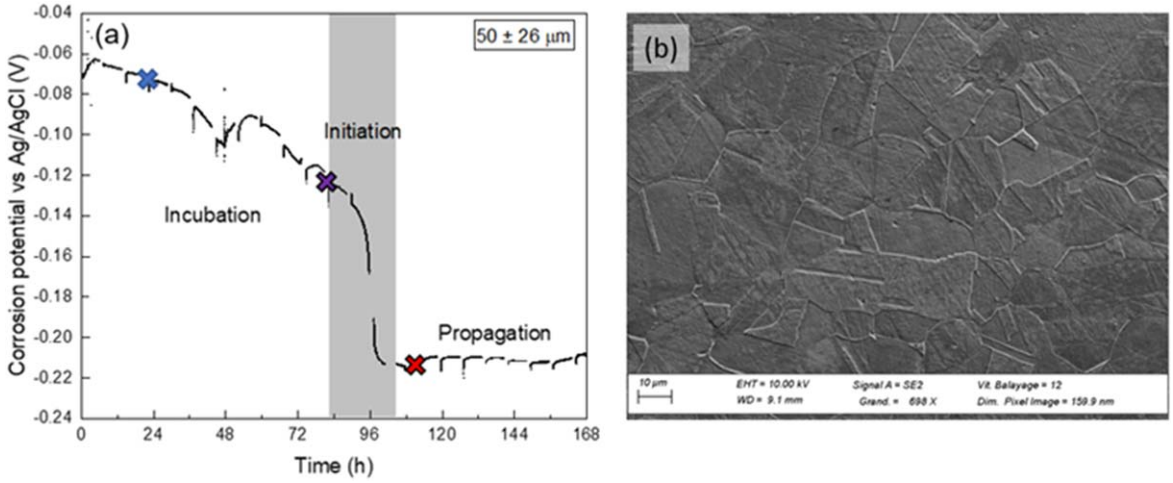

Figure 5. (a) Evolution of corrosion potential for NBA 825 immersed in 50 μm thin-layer of electrolyte (30 g L^{-1} NaCl solution acidified by H_2SO_4, configuration without probes) and (b) micrograph of the surface after 168 h of immersion.

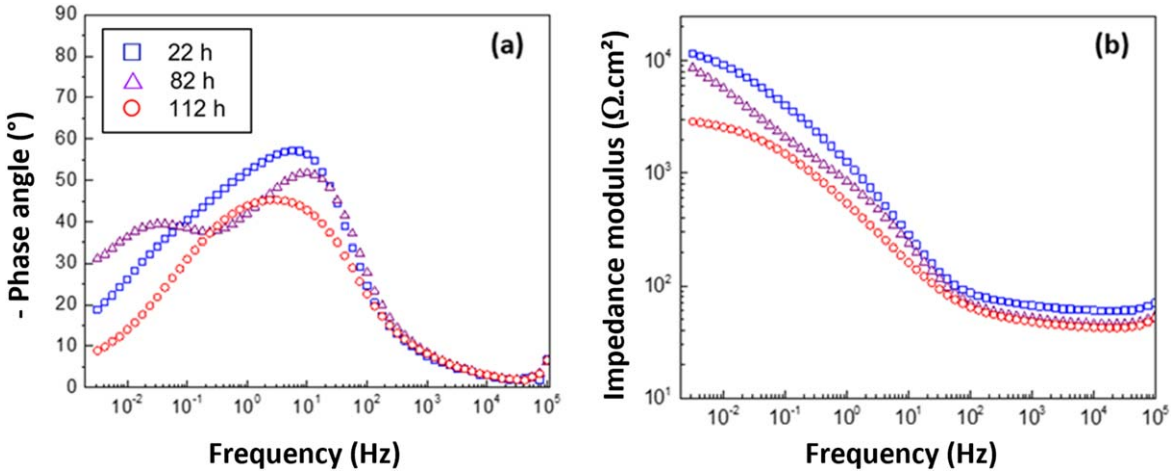

Figure 6. Electrochemical impedance diagrams, in Bode representation, obtained during immersion at corrosion potential for NBA 825 in thin-layer cell (50 μm ± 26 μm, 30 g L^{-1} NaCl at pH 0.5: (a) phase angle and (b) impedance modulus as a function of the frequency.

corresponding to the incubation period, the corrosion potential continuously decreased from −60 to −130 mV vs Ag/AgCl, then dropped during initiation and stabilized during propagation with a steady corrosion potential at −220 mV vs Ag/AgCl. Figure 5b shows SEM micrograph after 168 h of immersion at corrosion potential in the thin layer electrolyte. Under these conditions, it is mainly the grain boundaries that are sensitive to corrosion, as previously observed after the test in natural seawater (Fig. 1).

Figure 6 shows impedance diagrams obtained between 22 and 82 h, corresponding to the beginning and end of the incubation period and after 112 h during the propagation of the corrosion, marked in Fig. 5a. On the Bode diagrams, at least two-time constants can be observed at any time (Figs. 6a and 6b). The time constant exhibited between 1 and 10 Hz is characterized by a phase angle that decreases from 60° to 45° during immersion. The second time constant appears more clearly on the phase diagram at low frequency at the end of the incubation phase (Fig. 6a). For shorter immersion times, the two-time constants are overlapped. The low-frequency impedance modulus drops from 9×10^3 to 3×10^3 Ω cm^2 between the end of incubation and propagation confirms the decrease of the corrosion resistance of the working electrode during this stage of crevice corrosion (Fig. 6b).

It is important to underline that the geometry of the electrochemical cell affects the high-frequency part of the impedance diagrams.[28] Several models have been developed to accommodate the ohmic impedance caused by the cell geometry. The most suitable model in the present case is the Havriliak–Negami formula suggested by Gharbi et al.[28] It considers the frequency dispersion at the interface between a circular working electrode and the surrounding insulant, which will imply a current distribution. The Havriliak–Negami formula works for fitting a capacitive electrode, phase constant element (CPE), and in a state of active dissolution. It was also successfully used by Dizon et al. for an interdigitated electrode,[29] creating a thin layer of electrolyte between the working electrode and counter electrode. The Havriliak-Negami formula is given in Eq. 2, with R_{HF} and R_{LF} representing the "high" and "low" frequency electrolyte resistance, respectively:

$$z_{HN} = R_{HF} + \frac{R_{LF} - R_{HF}}{(1 + (j\omega T)^{\nu})^{\beta}} \quad [2]$$

It was demonstrated by Gharbi et al. that when used to describe CPE behavior, ν can be replaced by α accounting for the ideality of the capacitance (when $\alpha = 1$; otherwise, the layer is associated with a capacitance).[30] The parameter β is also used to account for the frequency dispersion, and T is the characteristic time constant of the ohmic impedance. The fitting of the high-frequency part of the Nyquist diagram for NBA 825 in a thin-layer of 50 ± 26 μm

thickness (in 30 g L^{-1} NaCl solution at pH = 0.5) after 22 h of immersion is presented in Fig. 7. From the fitting of the high-frequency part of the Nyquist diagram, it is obvious that considering only the electrolyte resistance (R_e = 57 Ω cm^2, graphically determined[30]) is not sufficient to accommodate the high-frequency phenomena (red curve). Using the Havriliak–Negami relation, the high-frequency part of the impedance diagram is well fitted, as observed in Fig. 7 (R_{HF} = 58 Ω cm^2, R_{LF} = 65 Ω cm^2, ν = 0.85, T = 1.9 10^{-4} s, and β = 0.65).

At the beginning of the immersion, the conditions allow to maintain the passive state of NBA 825 (pH close to 0.5 and content in dissolved O_2 close to 6 ppm, Figs. 4a and 4b, respectively). For longer immersion times, the severity of the environment (decrease in pH promoting an increase in [Cl^-]) leads to the loss of the film properties and thus to the dissolution of the alloy. Thus, the time constant at medium frequency can be attributed to the passive film response and at low frequency to the charge-transfer process (regarding the evolution of the impedance modulus at low frequency presented in Fig. 6b). However, it is important to note that the faradaic process is affected by the kinetics of diffusion of the dissolved electroactive species (mainly O_2), which is a limiting step in the thin-layer cell. Hence, this time constant is shifted toward lower frequencies (5 × 10^{-2} Hz) compared with those conventionally expected for charge transfer (0.1–1 Hz). From this understanding, an equivalent circuit is presented in Fig. 8. The low-frequency time constants are described using the charge transfer resistance (R_{ct}) and a double layer constant phase element (CPE_{dl}), and the medium-frequency time constant is attributed to the passive film resistance (R_f) and its constant phase element (CPE_f). Similar equivalent circuits have been previously proposed for stainless steel and nickel alloys in neutral and acidic environments.[31,32] The last part considers a complex ohmic impedance described below (Z_{HN}). It can be specified that a Warburg element was added in series to the charge transfer resistance to consider the oxygen diffusion in the thin-film electrolyte, but the extracted parameters were inconsistent. Thus, the choice was to describe the interface by the circuit presented in Fig. 8 by knowing that certainly the low frequency part of the impedance diagrams is more complex to model. The impedance of CPE parameter is given by Eq. 3. The CPE parameter α is an ideality factor; when its value is 1, the considered interface acts as a capacitor. The second CPE parameter Q is a pseudo-capacitance expressed as Ω^{-1} cm^{-2} sα.

$$Z_{CPE} = \frac{1}{Q(j\omega)^{\alpha}} \quad [3]$$

The fitted diagrams are presented in Fig. 9 and fit closely with the experimental data (the standard deviation, represented by red dashed line, covers a narrow range with experimental data). The fitted values are superposed with the experimental data in blue for all the steps of the crevice corrosion process. Table III presents the parameters extracted from the fitting for these three test durations and three supplementary ones to accurately monitor the evolution of the interface (45 h, 88 h, 116 h). All the fitted parameters have a confidence interval lower than 5%. At the beginning of the incubation phase, the parameter α_f is equal to 0.85 and decreases to 0.79 during propagation as the passive film is less stable and partially or totally dissolved. The value of α_{ct} is between 0.50 and 0.55, indicating that the CPE_{dl} is not only associated to the double layer capacitance but stands also for electroactive diffusion in the thin-layer cell. The value of Q_f increases at the end of incubation and during propagation, which is consistent with the decreasing of α_f. The parameter Q_{ct} increases during the incubation phase and then drops during propagation. It is important to mention that at OCP, anodic and cathodic reactions contribute to the impedance response of the working electrode. In the present case, the interface is intricate with the presence of passive film (partially dissolved) and cathodic reactions as oxygen reduction and proton reduction. The passive film resistance and the charge transfer resistance are stable during the

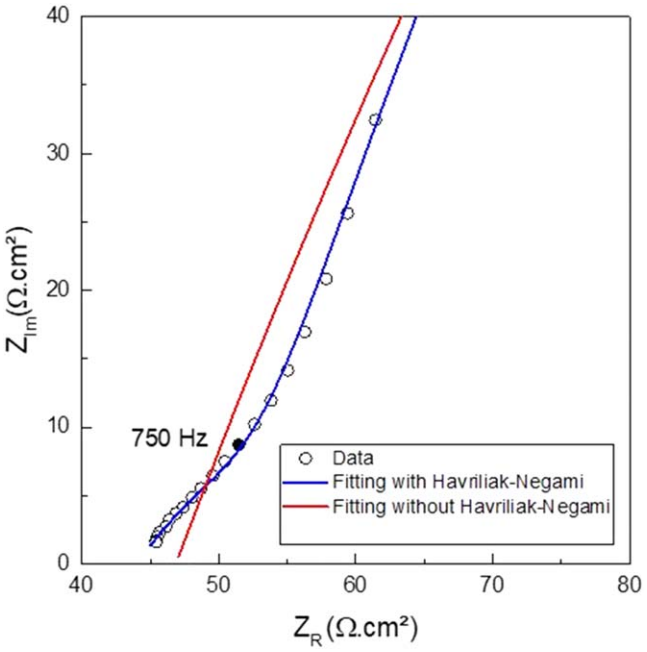

Figure 7. Adjustments of the high-frequency part of the Nyquist diagram obtained after 82 h of immersion under previous conditions.

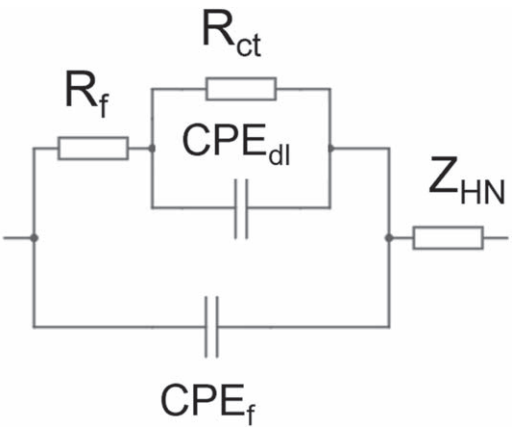

Figure 8. Electrical equivalent circuit suggested for adjustment of impedance diagrams obtained for NBA 825 in the thin-layer cell.

incubation time and drop directly before propagation. As these two values are closely linked from an electrochemical viewpoint (when the passive film is less resistant, the charge transfer increases), the polarization resistance (R_p), defined by the sum of resistances R_f and R_{ct} was considered.

The evolutions of R_{HF} (which is more significant than R_{LF} in the value of the Z_{HN} formula) and R_p as function of time are shown in Fig. 10. The values of the resistance attributed to R_{HF}, representative of the electrolyte resistance, decrease over time. This means that the electrolyte becomes more conductive because of the presence of more ionic species in solution. This result is attributed to chloride electromigration, solution acidification, and passive film dissolution, which are in accordance with the change of electrolyte chemistry as observed previously. The polarization resistance is almost stable between 16 and 23 kΩ cm^2 during the incubation period before a sharp decrease after 100 h of immersion. During propagation of corrosion, it remains at approximately 3 kΩ.cm^2. The duration after which the R_p significantly decreases corresponds to the open-circuit potential shift in the cathodic direction observed after 4 d (Fig. 5). Polarization resistance is also a good witness of sample behavior

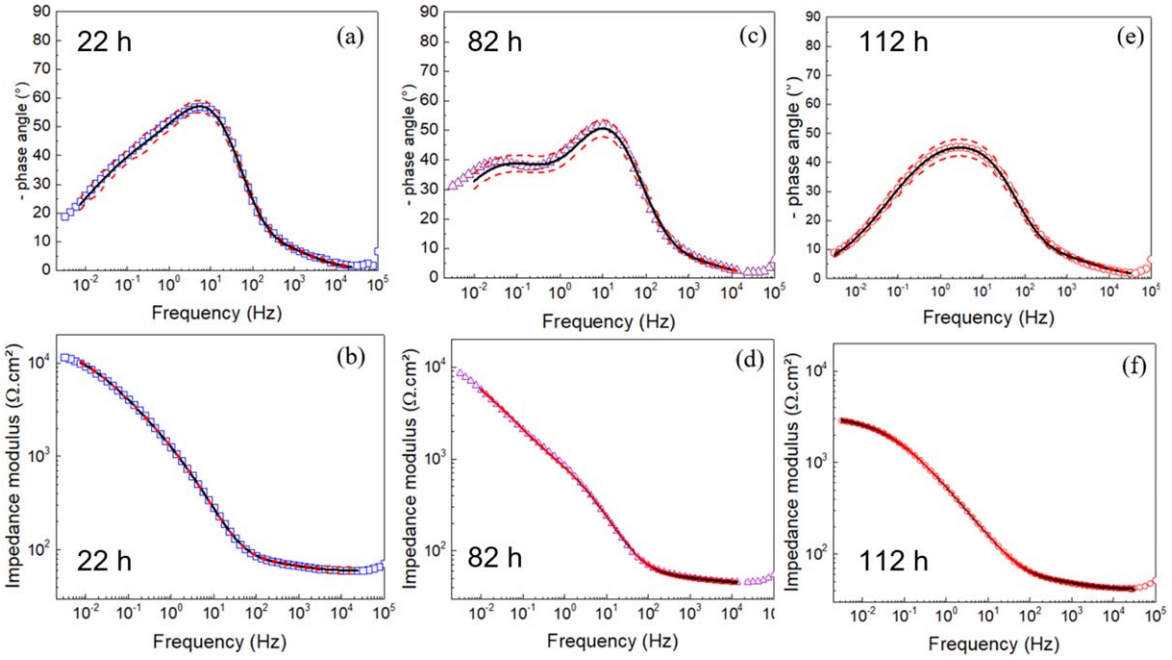

Figure 9. Adjustment of the experimental Bode impedance diagrams obtained over time: (a), (c), and (e) fitted phase angle and (b), (d), and (f) impedance modulus. The blue dots are experimental data, the yellow and red lines are the fitted results and the standard deviation, respectively.

during incubation and propagation stage which cannot be provided as precisely by OCP monitoring.

This analysis highlights that the electrochemical processes occurring in the thin-layer cell have been determined during all stages of crevice corrosion. This approach was used for different thin-layer thicknesses of electrolyte.

Limitation of cathodic reaction in the thin-layer cell.—Previous results show that the low-frequency part of the impedance diagrams is due to the cathodic reaction, which evolves over time:

- During incubation, the reduction reaction is mixed, due to the contribution of dissolved O_2 (as shown in Fig. 4b) and proton due to the intial pH of the electrolyte,

When dissolved oxygen is consumed, the reduced species is the proton.

To avoid this contribution to the electrochemical signal, a graphite electrode immersed in a neutral NaCl 30 g L^{-1} solution was offset from the thin film and coupled to NBA 825, which is in contact with the thin electrolyte film. In this way, the coupling enables the cathodic and anodic sites to be dissociated on the graphite and alloy studied, respectively. For corrosion potential measurements, the cathode and anode were physically coupled, constituting the working electrode. As previously shown, electrochemical impedance measurements were carried out on the thin-film material by decoupling it from the cathode. It was verified experimentally that the decoupling time does not alter the electrochemical behavior of the anode. Figure 11 shows that the shape of the impedance diagrams differs according to the electrochemical cell configuration used. The phase diagram shows a widening of the mid-frequency time constant, attributed to the passive film, and a disappearance of the low-frequency time constant attributed to charge transfer, suggesting that the charge transfer contribution is limited.

Figure 12 shows the impedance diagrams obtained over time for NBA 825 in contact with the 50 μm-thick stagnant electrolyte film. The value of the low-frequency impedance modulus decreases by a factor of 10 between 12 h and 40 h of immersion, reaching 2 kΩ cm^2. These changes show a shorter incubation time, leading to a faster decrease in the corrosion resistance of the anode than in the previous configuration. In parallel, the phase versus frequency

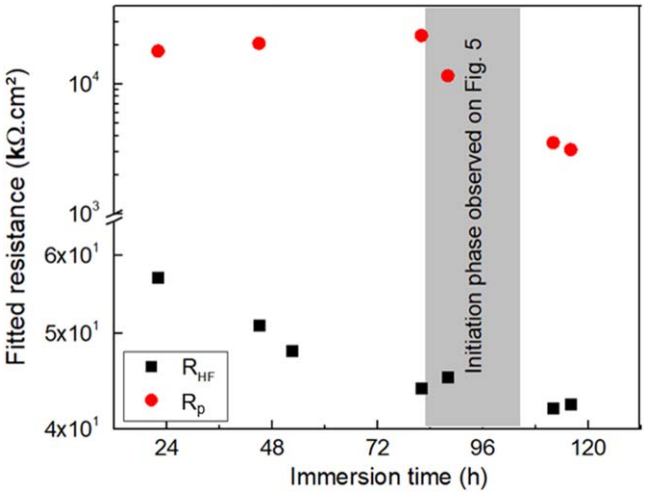

Figure 10. Evolutions of polarization resistance (R_p) and electrolyte resistance (R_{HF}) for the NBA 825 in contact with a 50 ± 26 μm thick film of acidic sodium chloride solution electrolyte.

diagram changes. This indicates that the kinetics of metal cation hydrolysis and chloride ion electro-migration are accelerated under these conditions. The equivalent electrical circuit shown in Fig. 12c was used to obtain parameter trends. A single R//CPE element was sufficient to adjust the diagrams, with R the resistance of the passive film and CPE the Constant-Phase-Element attributed to the passive film that becomes, during immersion, a charge-transfer resistance and a double-layer pseudo-capacitance, respectively. Table IV summarizes the results of the adjustment. In comparison with the data in Table III, the reduction process has an effect on the resistance values attributed to the passive film: 3 kΩ cm^2 after 80 h for the previous configuration, whereas with the new configuration, this resistance value is reached after 40 h of immersion. All these results with this new configuration show the effect of the cathodic process on low frequencies. However, whatever the configuration used and once the processes have been established, the parameters become comparable.

Table III. Parameters extracted from the adjustment of the impedance diagrams obtained during immersion time.

Time/h	$R_{HF}/\Omega\ cm^2$	$R_{LF}/\Omega\ cm^2$	β	$T/10^{-4}$ s	α_f	$Q_f/10^{-4}\ \Omega^{-1}\ cm^{-2}\ s\alpha$	$R_f/10^3\ \Omega\ cm^2$	α_{dl}	$Q_{dl}/10^{-4}\ \Omega^{-1}\ cm^{-2}\ s\alpha$	$R_{ct}/10^3\ \Omega\ cm^2$	$R_p/10^3\ \Omega\ cm^2$
22	58	69	0.65	1.9	0.85	1.1	16.6	0.50	2.6	1.3	18.0
45	51	62	0.62	2.2	0.85	1.1	19.5	0.50	4.0	1.1	20.6
82	44.0	52.1	0.67	1.6	0.83	1.4	22.7	0.54	6.9	0.8	23.4
88	42.5	50.0	0.70	1.0	0.81	1.7	11.0	0.55	14	0.6	11.6
112	42.4	51.6	0.65	2.8	0.79	2.2	3.4	0.50	5.0	0.2	3.5
116	42.0	48.4	0.65	1.0	0.79	2.0	3.0	0.50	4.0	0.1	3.1

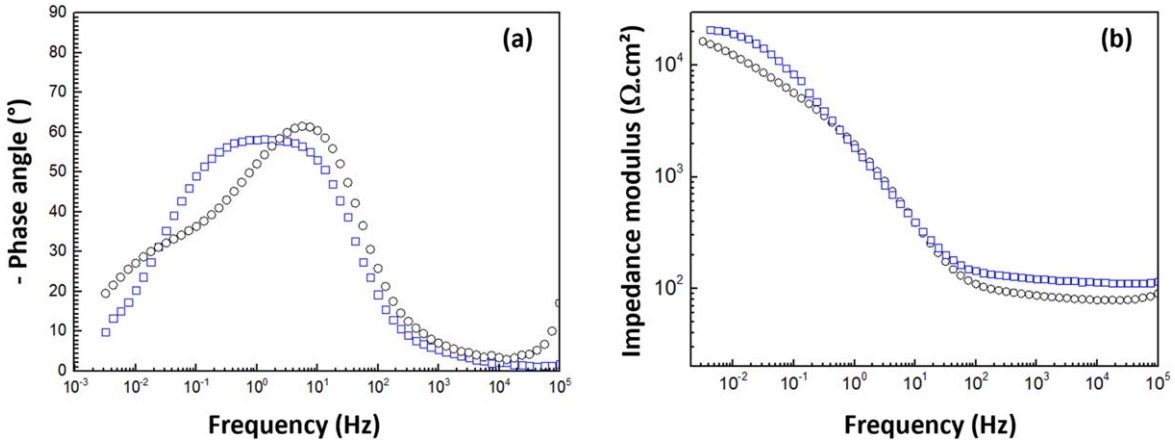

Figure 11. Electrochemical impedance diagrams, in Bode representation, obtained after 12 h of immersion in the thin-layer cell for the configuration: (◯) without and (□) with the deported cathode. The electrolyte thickness was 50 μm ± 15 μm.

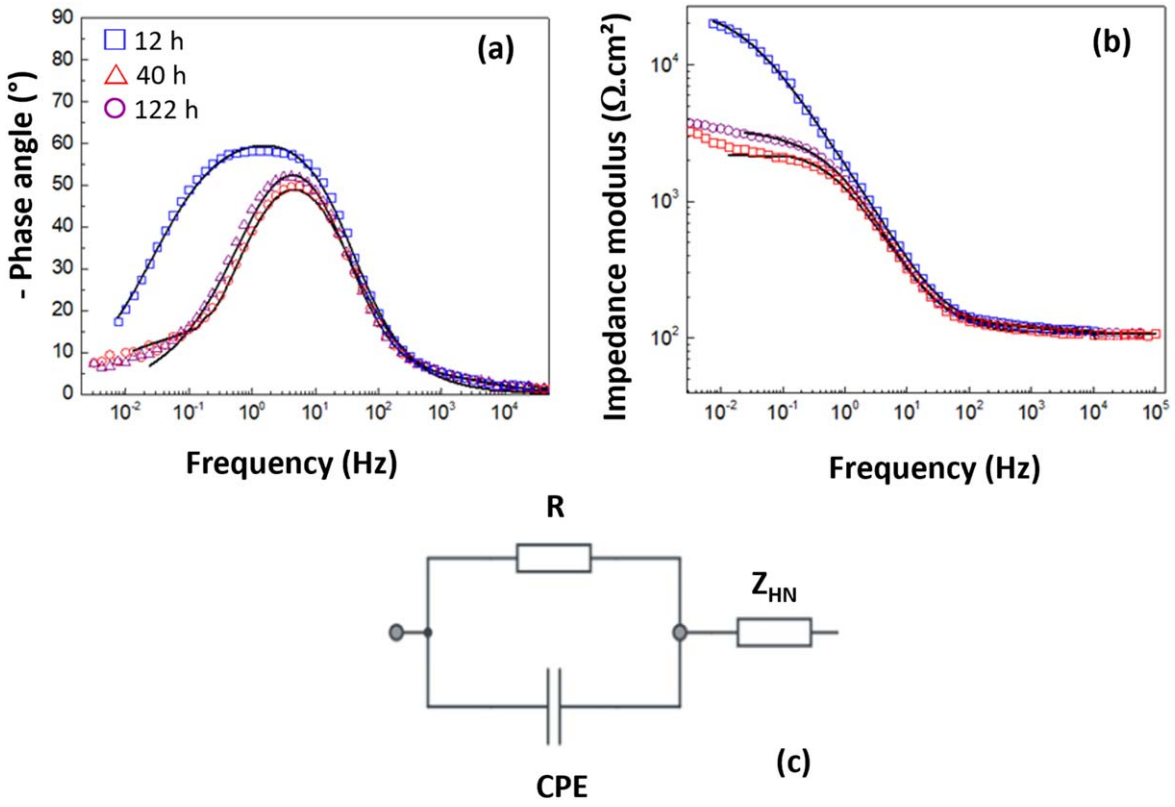

Figure 12. Electrochemical impedance diagrams obtained during time for the NBA in contact with the thin film of electrolyte (50 μm ± 15 μm): (a) phase and (b) impedance modulus as a function of frequency fitted by (c) electrical equivalent circuit.

Table IV. Fitted parameters from impedance diagrams obtained during time for the configuration with deported cathode. The film thickess of electrolyte in contact with the NBA 825 was 50 μm ± 15μm.

	Z_{HN}						
Time/h	R_{HF}/Ω cm^2	R_{LF}/Ω cm^2	β	T/10^{-4} s	α	Q/$10^{-4}\Omega^{-1}$ cm^{-2} sα	R/$10^3\Omega$ cm^2
12	100	120	0,84	0,65	0,75	1,41	23,8
40	105	112	0,82	1,0	0,75	1,55	3,2
71	105	130	0,82	1,0	0,79	1,41	2,4
120	100	114	0,75	0,74	0,79	1,40	2,2

Finally, whatever the configuration chosen, the same phenomena in the thin-layer cell led to the physico-chemical conditions that lead to the development of crevice corrosion. When the first configuration is used (without moving the cathodic reaction), cathodic reactions take place within the thin film and slow down the establishment of these conditions. However, once O_2 depletion has occurred, proton reduction still takes place. However, this does not alter the conditions that lead to chemical depassivation of the alloy.

Conclusions

To investigate the electrochemical behavior of alloy 825 during crevice corrosion, an improved thin-layer cell was developed permitting the in situ measurement of the dissolved O_2 content and the pH. The main advantage of this development is to monitor the reactivity of the material over time regarding the thin-film electrolyte chemistry evolution as opposed to post-mortem observation of the corrosion attacks at the end of experiments.

The choice of the starting electrolyte and the electrolyte film thickness conditions the incubation time. To decrease this period, a pH 0.5 (slightly superior to the depassivation pH) solution was used.

The evolution of the impedance diagrams was discussed with respect to the evolution of the corrosion potential and the modification of the electrolyte in the confined area. An equivalent electrical circuit was proposed to fit the experimental diagrams. The electrochemical response related to charge transfer and passive film is closely linked to cathodic reduction processes: mixed reduction of dissolved oxygen and proton, then only proton when dissolved O_2 is consumed. To avoid the reduction reaction of dissolved oxygen on the surface of the NBA 825 in contact with the thin film of stagnant electrolyte, a graphite cathode was placed outside the thin-layer cell and bought into contact with a neutral chloride solution. Results showed that incubation time was significantly reduced. However, once the incubation period was reached, the use of this set-up did not modify the electrochemical behavior of the study material acting as anode. Thus, the evolution of the polarization resistance, which decreases significantly as the severity of the electrolyte contained in the confined zone increases over time due to the crevice corrosion process, is correlated to the variation in corrosion potential. On the other hand, polarization resistance monitoring appears to be more accurate than corrosion potential monitoring as the material moves from the passive state (incubation period) to the active state (corrosion initiation and propagation). This finding highlights the contribution of impedance measurement compared to corrosion potential measurement.

This work demonstrates the versatility of the thin-film cell to reproduce an environment encountered during the setting up of crevice corrosion (without forcing electrochemical processes) and to study the electrochemical behavior of a passive material under such conditions. The developed methodology can be used for further study of corrosion mechanisms for other materials and also allows a classification of alloys.

References

1. N. Sridhar, R. Thodla, F. Gui, L. Cao, and A. Anderko, *Corros. Eng. Sci. Technol.*, **53**, 75 (2018).
2. A. Al-Odwani, J. Carew, and A. Al-Hashem, *CORROSION 99. Paper*, 326 (1999).
3. H. Alves and M. S. Niederau, *CORROSION 2008, paper*, 08259 (2008).
4. J. Botinha, B. Gehrmann, M. Wolf, and H. Alves, *CORROSION 2021* (2021), paper Number: NACE-2021-16398.
5. J. Botihna, M. Wolf, and H. Alves, *AMPP Annual Conference + Expo, paper Number: AMPP-2023-18847* (2023).
6. D. S. Bergstrom, S. M. Nacéra, and J. D. John, (2021)paper NACE-2021-16555CORROSION 2021.
7. 'Standard Test Methods for Pitting and Crevice Corrosion Resistance of Stainless Steels and Related Alloys by Use of Ferric Chloride Solution'. ASTM G48-11 (2020)e1.
8. 'Standard Guide for Crevice Corrosion Testing of Iron-Base and Nickel-Base Stainless Alloys in Seawater and Other Chloride-Containing Aqueous Environments'. ASTM G78-20.
9. L. Stockert and H. Böhni, *Mater. Sci. Forum*, **44-45**, 313 (1989).
10. S. Azuma, T. Kudo, H. Miyuki, M. Yamashita, and H. Uchida, *Corros. Sci.*, **46**, 2265 (2004).
11. H. Baba and Y. Katada, *Corros. Sci.*, **48**, 2510 (2006).
12. R. S. Lillard, S. Mehrazi, and D. M. Miller, *J. Electrochem. Soc.*, **167**, 141503 (2020).
13. N. S. Zadorozne, C. M. Giordano, M. A. Rodriguez, R. M. Carranza, and R. B. Rebak, *Electrochim. Acta*, **76**, 94 (2012).
14. Standard Guide for Crevice Corrosion Testing of Iron-Base and Nickel-Base Stainless Alloys in Seawater and Other Chloride-Containing Aqueous Environments, G78-01 (2007).
15. S. T. Arab, K. Emran, H. M. Alghamdi, and M. H. Abdulsalam, *International Scientific Research Journal*, **1**, 17 (2015).
16. Q. Hu, G. Zhang, Y. Qiu, and X. Guo, *Corros. Sci.*, **53**, 4065 (2011).
17. W. Xu, Y. Deng, B. Zhang, J. Zhang, Z. Peng, B. Hou, and J. Duan, *Mater. Res. Technol.*, **16**, 1856 (2022).
18. L. Yan, G.-L. Song, Z. Wang, and D. Zheng, *Constr Build Mater*, **296**, 123587 (2021).
19. C. Fiaud, M. Keddam, A. Kadri, and H. Takenouti, *Electrochim. Acta*, **32**, 445 (1987).
20. M. Keddam, A. Hugot-Le-Goff, H. Takenouti, D. Thierry, and M. C. Arevalo, *Corros. Sci.*, **33**, 1243 (1992).
21. C. Gabrielli, M. Keddam, N. Portail, P. Rousseau, H. Takenouti, and V. Vivier, *J. Phys. Chem. B.*, **110**, 20478 (2006).
22. E. Remita, B. Tribollet, E. Sutter, V. Vivier, F. Ropital, and J. Kittel, *Corros. Sci.*, **50**, 1433 (2008).
23. S. Marcelin, N. Pébère, and S. Regnier, *J. Electroanal. Chem.*, **737**, 198 (2015).
24. T. P. Hoar, D. C. Mears, and G. P. Rothwell, *Corros. Sci.*, **5**, 279 (1965).
25. E. Remita, E. Sutter, B. Tribollet, F. Ropital, X. Longaygue, C. Taravel-Condat, and N. Desamais, *Electrochim. Acta*, **52**, 7715 (2007).
26. W. Watson and M. Orazem, *EIS: Measurement Model Program*, v1**4** (2020).
27. J.-L. Crolet, L. Seraphin, and R. Tricot, *Matériaux & Techniques*, **66**, 355 (1978).
28. O. Gharbi, A. Dizon, M. E. Orazem, M. T. T. Tran, B. Tribollet, and V. Vivier, *Electrochim. Acta.*, **320**, 134609 (2019).
29. A. Dizon and M. E. Orazem, *Electrochimi. Acta.*, **327**, 135000 (2019).
30. M. E. Orazem, N. Pébère, and B. Tribollet, *J. Electrochem. Soc.*, **153**, B129 (2006).
31. C. M. Fernandes, A. Rocha, J. P. Cardoso, A. C. Bastos, E. Soares, J. Sacramento, M. G. S. Ferreira, and A. M. R. Senos, *Int. J. Refract. Met. H.*, **72**, 21 (2018).
32. R. F. Santos et al., *Int. J. Refract. Met. H.*, **95**, 105434 (2021).